Precambrian Research 168 (2009) 259–270

Contents lists available at ScienceDirect

Precambrian Research

journal homepage: www.elsevier.com/locate/precamres

Oceanic redox conditions in the Late Mesoproterozoic recorded in the upper Vazante Group carbonates of São Francisco Basin, Brazil: Evidence from stable isotopes and REEs

Karem Azmy[a,*], Paul Sylvester[a], Tolentino F. de Oliveira[b]

[a] Department of Earth Sciences, Memorial University of Newfoundland, St. John's, NL, A1B 3X5 Canada
[b] Votorantim Metais, P.O. Box 03, 38780-000 Vazante MG, Brazil

ARTICLE INFO

Article history:
Received 3 January 2008
Received in revised form 10 October 2008
Accepted 14 October 2008

Keywords:
Vazante carbonates
Brazil
REE
Th/U
Redox conditions

ABSTRACT

The Vazante Group consists of a late Mesoproterozoic (~1.0–1.1 Ga) carbonate-dominated marine platform sequence in east-central Brazil. The upper part of the sequence consists of a glaciomarine diamictite unit overlain by a cap carbonate. The $\delta^{13}C$ profile of the upper Vazante shows significant negative plunges, one preglacial (drop of ~5.5‰ VPDB) and two postglacial (drops of ~9 and 5‰VPDB, respectively). The C-isotope plunge in the preglacial carbonates is correlated with low Th/U ratios (0.1–1.4) and a negative Ce/Ce* shift (~0.4), suggesting deposition under relative reducing conditions. In contrast, the C-isotope plunges in the postglacial carbonates are associated with high Th/U ratios (>2) and positive Ce/Ce* shifts (up to ~1.5), thus reflecting oxidizing conditions. Variations in the redox conditions of the late Mesoproterozoic ocean, reflected by changes in the Th/U and Ce/Ce* ratios, are likely attributable to a combination of both global and local climatic and oceanographic changes, similar to what has been inferred for the Neoproterozoic oceans.

1. Introduction

Preserved marine carbonates are known to retain their primary chemical, elemental and isotopic, signatures that reflect the effect of prevailing oceanographic conditions and patterns (e.g., Wignall and Twitchett, 1996; Shields et al., 1997; Azmy et al., 1998; Veizer et al., 1999; Arnaboldi and Meyers, 2007; Wignall et al., 2007). Anoxic conditions have a dramatic impact on the organic productivity in oceans and, in most cases, may result in global mass extinction events (e.g., Wignall and Twitchett, 1996). Although anoxic events in the Phanerozoic oceans developed mainly in stratified oceans, the Neoproterozoic anoxia is believed to have been caused by extensive global glaciation that reached as far as the equatorial latitudes (Snowball Earth hypothesis) and the ice cover separated the ocean from atmosphere, thus resulting in severe drop in oxygen levels in sea surface waters (Hoffman et al., 1998; Hoffman and Schrag, 2002). These events were usually associated with the deposition of glaciogenic marine diamictites with dropstones and likely resulted in significant reduction in organic primary productivity and high rate of burial of organic carbon (cf. Halverson et al., 2005 and more references therein). The termination of glaciation left behind ^{12}C-depleted surface waters to recover productivity, which is reflected by the negative $\delta^{13}C$ shifts exhibited in the cap carbonates immediately above the glaciogenic diamictites (e.g., Halverson et al., 2005, 2007). On the other hand, the redox conditions influence the oxidation state and solubility of some rare earth elements (REEs) in ocean water such as Ce, and U, relative to other elements that stay unaffected such as Th (e.g., Wignall and Twitchett, 1996; Shields et al., 1997).

Redox variations in the oceans prior to the Neoproterozoic have been the subject of some recent investigations (e.g., Kah et al., 1999; Schen et al., 2002, 2003; Arnold et al., 2004; Brocks et al., 2005) but remain poorly known and are worthy of further study. Thus, it is of some interest that remarkable negative $\delta^{13}C$ shifts have been documented in cap carbonates of the upper Vazante Group diamictites of east-central Brazil (Azmy et al., 2001, 2006), which has recently been determined to have formed in the late Mesoproterozoic (Azmy et al., 2008). The current investigation presents evidence from Th, U and other REE variations in the carbonates to evaluate the redox conditions associated with the glacial event that formed them.

2. Geologic setting and age constraints

The Vazante Group consists of a carbonate-dominated marine platform sequence (Dardenne, 2001) that extends along more than 300 km N-S in the external zone of the Brasilia Fold Belt in São

* Corresponding author. Tel.: +1 709 737 6731; fax: +1 709 737 2589.
E-mail address: kazmy@mun.ca (K. Azmy).

0301-9268/$ – see front matter © 2008 Elsevier B.V. All rights reserved.
doi:10.1016/j.precamres.2008.10.003

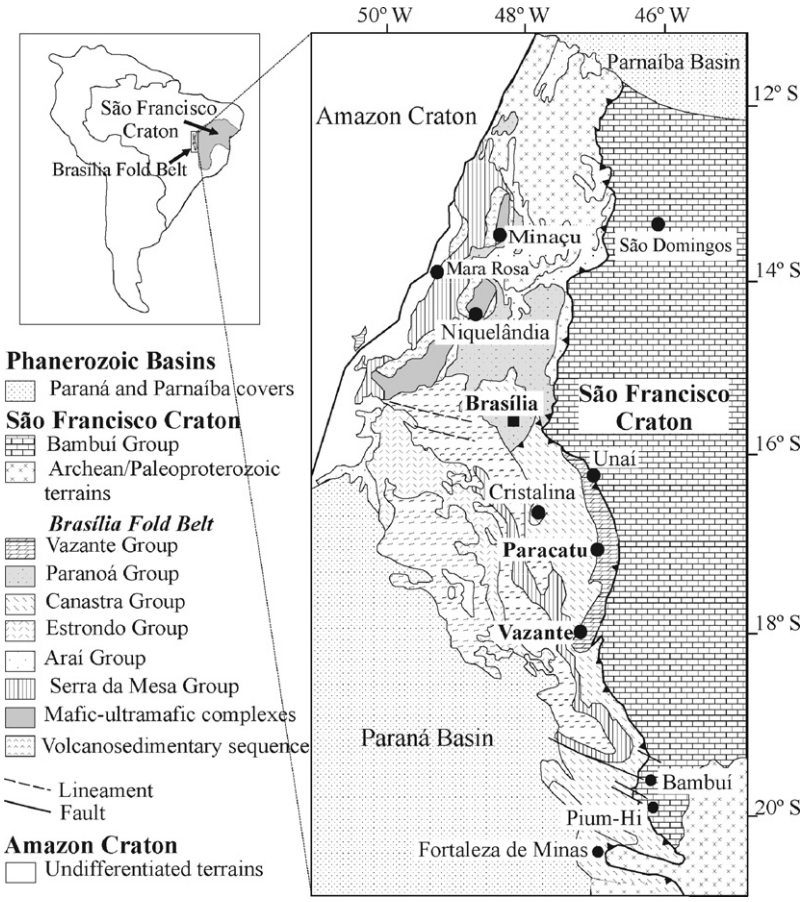

Fig. 1. Location map of São Francisco Basin in Brazil showing the geology of the Brasilia Fold Belt including the Vazante Group (modified from Valeriano et al., 2004).

Francisco Basin (Fig. 1). The stratigraphy of the marginal marine sediments of the Vazante Group (Fig. 2) has been studied in detail and refined by several authors (e.g., Dardenne, 1978; Dardenne and Walde, 1979; Madalosso, 1979; Karfunkel and Hoppe, 1988; Fairchild et al., 1996; Azmy et al., 2001, 2006; Dardenne, 2001; Misi, 2001; Misi et al., 2007). Sediments in the eastern part of the basin are generally preserved but they become highly deformed and metamorphosed (amphibolite to granulite facies) to the west near the Brazilia Fold Belt (Dardenne, 1978; Fuck et al., 1994). Earlier studies indicated that the Vazante Group sediments accumulated on a passive margin (e.g., Campos-Neto, 1984; Fuck et al., 1994), but recent investigations suggest that these sediments were deposited in a foreland basin during the initial phases of the Brasiliano orogeny (e.g., Dardenne, 2000) although the lack of evidence of volcanic activity (ash layers) in the sequence would favor the former model rather than the latter.

The Vazante Group is believed to rest on a glaciogenic unit (D), which constitutes the top of the Santo Antônio do Bonito Formation (Fig. 2) and includes another glacial horizon (D II) near the top of the succession (Olcott et al., 2005) at the base of the Lapa Formation (Azmy et al., 2006). Sedimentary iron-formation and iron-oxide cemented diamictites are also observed near the top of this second glaciogenic interval (Brody et al., 2004). A regional unconformity (Fig. 2) likely occurs at the base of the upper diamictite (D II) throughout the entire basin (Misi et al., 2007).

The Vazante Group stratigraphic framework is summarized in Fig. 2. Remarkable $\delta^{13}C$, and REE, variations have been documented mainly in the upper part of the Group below and above the upper diamictite unit (D II) immediately below the Lapa Formation. The preglacial shifts are correlated with beds consisting mainly of pink dolomitized fenestral algal mats (microbialites) and bioherms of columnar stromatolites. On the other hand, the postglacial shifts above the diamictites (D II) are correlated with dolomitized carbonate rhythmites of the Lapa Formation.

The Lapa Formation, which overlies the younger diamictites (D II), is predominantly composed of rhythmically laminated argillaceous dolomites (cf. Azmy et al., 2006), with shales in the upper part (Fig. 3). Immediately above the upper Vazante Group diamictite (D II), thick organic-rich shale with dropstones (Azmy et al., 2006) deposited likely during postglacial transgression (Brody et al., 2004). The Lapa sediments represent a cap carbonate of subtidal laminated dolomitized lime mudstone alternating with clays or shales forming rhythmites (Azmy et al., 2006), which shallow upward to rhythmically bedded argillaceous dolomite and microbialaminite as well as occasional stromatolite lenses that likely deposited within the photic zone (Fig. 3).

Petrographic examination of thin sections shows that the dolomicrites are generally fabric retentive and very fine grained (Azmy et al., 2006) with no significant increase in crystal size associated with dolomitization, suggesting no extensive and/or repeated meteoric alteration.

The lack of volcanic ash layers and the absence of radiometric age estimates have made the age of the Vazante Group a matter of some debate. Previous chemostratigraphic studies of the C-isotope and $^{87}Sr/^{86}Sr$ (least radiogenic signature 0.706841) profiles of the Group, particularly those from the Lapa carbonates, suggested a possible correlation with similar isotopic profiles of Sturtian (800–650 Ma) sequences on the Congo Craton (Azmy et al., 2001, 2006; Misi et al., 2007). However, the recent radiometric measurements of Azmy et al. (2008) suggest an age of between

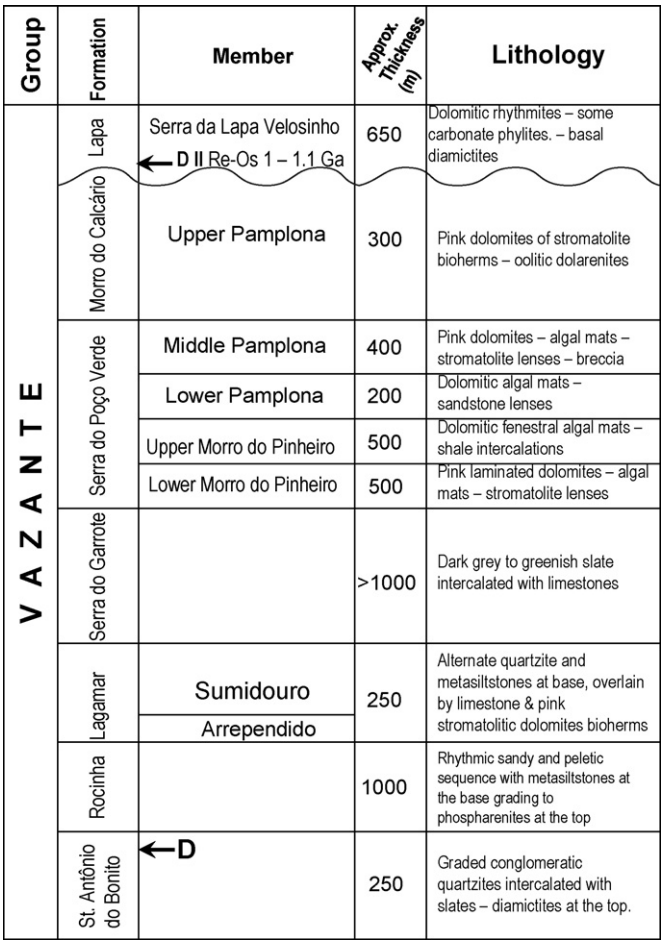

Fig. 2. Schematic diagram of the Vazante Group stratigraphy showing the positions of the glacial intervals, (D) at the top of Santo Antônio do Bonito Formation and (D II) at the base of Lapa Formation (modified from Dardenne, 2001).

1.0 and 1.1 Ga for the Vazante Group. Organic-rich shale associated with the diamictites at the base of the Lapa Formation has a Model 3 Re–Os isochron age of 1100 ± 77 Ma (Fig. 3). Also, Geboy (2006) obtained Re–Os ages of 1353 ± 69 Ma for organic-rich shales of the preglacial Serra do Garrote and glaciogenic Serra do Poço Verde Formations (middle Vazante Group, Fig. 2), respectively, that are consistent with the late Mesoproterozoic age determined by Azmy et al. (2008). In addition, Kaufman et al. (2008) documented successive isochron ages for the Serra do Garrote and Serra do Poço Verde formations between 1353 ± 69 Ma and 1126 ± 47 Ma. The Vazante $\delta^{13}C$ profile has negative shifts of up to 8‰ VPDB associated with absolute-age controlled organic-rich shale immediately above a glaciogenic interval (1.0–1.1 Ga). Previous studies documented Mesoproterozoic $\delta^{13}C$ profiles showing negative shifts of 4–6‰ VPDB, but have very poor absolute age control and were not associated with glaciogenic units (e.g., Kah et al., 1999; Bartley et al., 2007).

3. Methodology

A summary of the methods is described below. The analytical protocol of the trace element and stable isotope measurements (carbon and oxygen) on carbonates and organic matter has been explained in detail in Azmy et al. (2001, 2006).

Samples were collected at high resolution from cores (CMM244, CMM279, CMM500, and MASW01) covering the upper Vazante Group (Azmy et al., 2001, 2006), which were provided by the Brazilian mining company Votorantim Metais (Appendix A). Thin sections of the samples were petrographically examined under a standard polarizing microscope and cathodoluminoscope and stained with Alizarin Red-S and potassium ferricyanide solutions (Dickson, 1966). A mirror-image polished slab of each thin section was also prepared and polished for microsampling. Slabs were washed with de-ionized water and dried overnight at 50 °C prior to the isolation of the finest grained micrites free of secondary cements. Approximately, 4 mg were extracted under a binocular microscope from the slabs with a low-speed microdrill. The C- and O-analyses were run by reacting about 250 μg of powder sample in inert atmosphere with concentrated (100%) orthophosphoric acid at 70 °C in a Thermo-Finnigan Gasbench II. The CO_2 produced from the reaction was automatically delivered to a ThermoFinnigan DELTA V plus isotope ratio mass spectrometer, where the gas measured for isotope ratios. The uncertainty is better than 0.1‰ (2σ), based on repeated measurements of NBS-19 ($\delta^{18}O = -2.20$‰ and $\delta^{13}C = +1.95$‰ vs. V-PDB) and NBS-18 ($\delta^{18}O = -3.00$‰ and $\delta^{13}C = -5.00$‰ vs. V-PDB) standards during each run of samples (cf. Azmy et al., 2006).

For elemental analyses, a subset of sample powder was digested in 5% (v/v) acetic acid for 70–80 min to eliminate leaching the detrital silicate inclusions and analysed by standard addition techniques for major (e.g., Ca, Mg), minor (e.g., Sr, Mn), and REE (Coleman et al., 1989) using a HP 4500*plus* ICP-MS at Memorial University of Newfoundland. The relative uncertainties of these measurements are better than 5% (cf. Azmy et al., 2006). Normalization of Ce concentrations is based on the PAAS values (Post-Archean Australian Shale, McLennan, 1989) and the equation $Ce/Ce^* = 3(Ce/Ce\ PAAS)/\{(2La/La\ PAAS) + (Nd/Nd\ PAAS)\}$ (e.g., Shields et al., 1997).

Organic carbon isotope ratios were measured on isolated kerogen after repeated digestion with ultrapure concentrated hydrochloric acid at the isotope laboratory of Memorial University of Newfoundland, using a Carlo Erba Elemental Analyzer coupled to a 252 Finnigan Mat Mass Spectrometer. The results were normalized to the standards IAEA-CH-6 ($\delta^{13}C = -10.43$), NBS18 ($\delta^{13}C = -5.04$) and USGS24 ($\delta^{13}C = -15.99$) and the uncertainty calculated from repeated measurements was ~0.2‰ (cf. Azmy et al., 2006).

4. Results and discussion

4.1. Sample preservation

The degree of preservation of the Vazante carbonate samples of the current study was previously discussed in detail by Azmy et al. (2001, 2006) and carefully evaluated through a screening procedure, which involved several petrographic and geochemical techniques (e.g., Kaufman et al., 1991, 1992, 1993; Derry et al., 1992; Narbonne et al., 1994; Misi and Veizer, 1998). Thin sections were studied under a petrographic microscope to examine the grain size, recrystallization, detrital and organic contents and sedimentary structures and they were also examined under cathodoluminoscope. Only micritic material, usually exhibiting dull luminescence (cf. Rush and Chafetz, 1990), was microsampled under a binocular microscope from polished slabs, which are mirror images of the screened thin sections. The extracted powder was run for C- and O-isotopes, major and minor elements and REEs. The lack of correlations of Mn/Sr ratios with $\delta^{13}C_{carb}$ ($R^2 = 0.008$) and $\delta^{18}O$ ($R^2 = 0.001$) values (Fig. 4a,b) suggest a high degree of preservation of the $\delta^{13}C$ signatures likely because the diagenetic fluids do not contain much of CO_2 to reset the $\delta^{13}C$ signature of carbonates. The

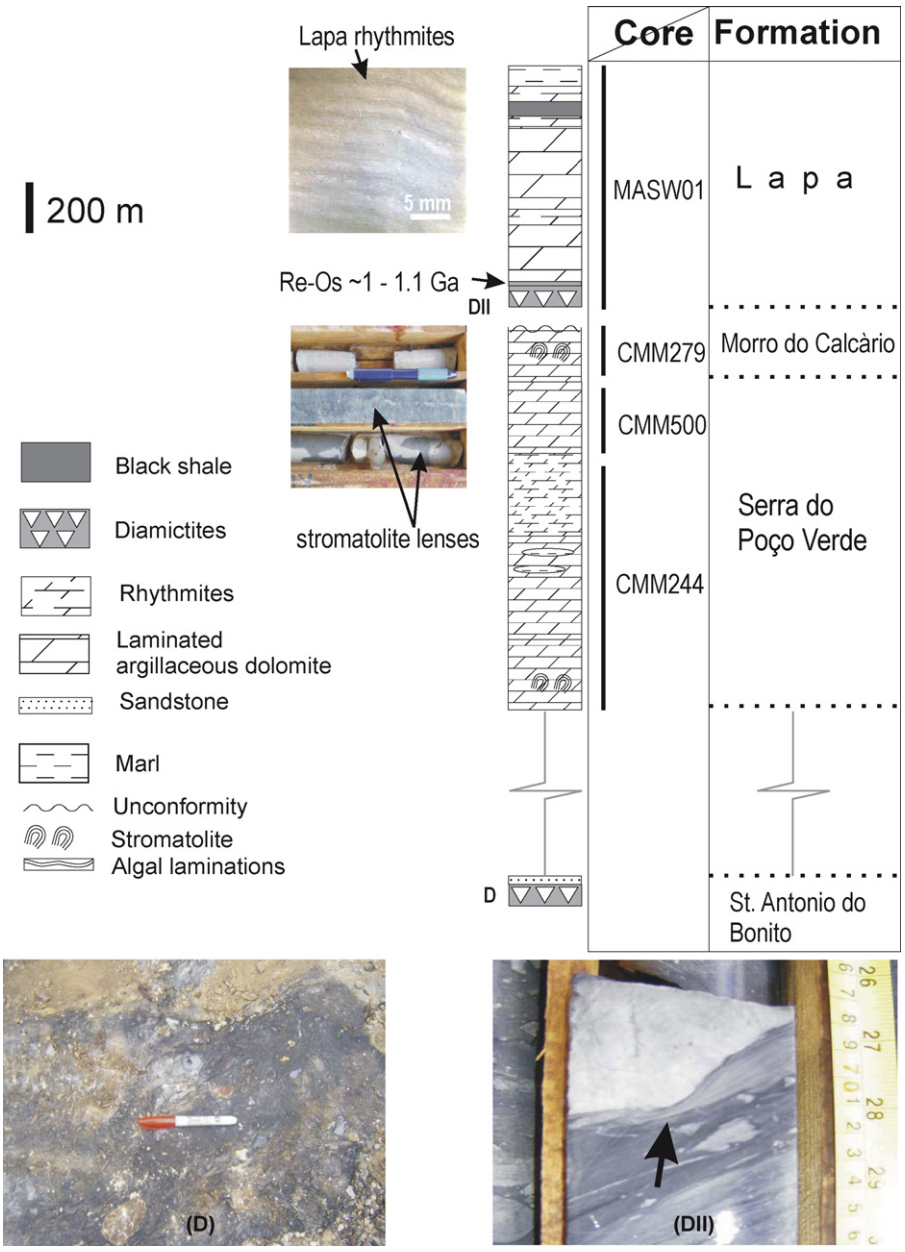

Fig. 3. Diagram showing a composite stratigraphic log of the upper Vazante Group with the stratigraphic positions of the basal and upper diamictites. Sampled cores are indicated next to each interval (cf. Azmy et al., 2001, 2006 for details). Radiometric age estimates are from Azmy et al. (2008). Photos at the bottom refer to the glaciogenic intervals D (lower most diamictite) and D II (upper diamictite with arrow pointing at a dropstone) and those at the top refer to the Lapa rhythmites and Morro do Calcàrio and Serra do Poço Verde stromatolite lenses, respectively.

organic matter isolated from the investigated carbonate samples has a range of $\delta^{13}C_{org}$ values between −26 and −13‰. Metamorphism may result in enrichment in the $\delta^{13}C_{org}$ (Schidlowski et al., 1975; Hayes et al., 1983; Holser et al., 1988; Hayes et al., 1999) but the lack of correlation between the C-isotope enrichment and organic carbon abundance (TOC) in the upper Vazante carbonates (Fig. 4c) would strongly argue against a metamorphic artifact (cf. Azmy et al., 2006). The $\delta^{13}C_{org}$ values show a parallel trend to that of $\delta^{13}C_{carb}$ (Fig. 5), which implies that the $\delta^{13}C_{carb}$ trend is likely primary, and that the variations in $\delta^{13}C_{org}$ are also primary, and it reflects changes in primary productivity in the depositional setting (cf. Azmy et al., 2006 for more details).

The Th/U and Ce/Ce* ratios of the Vazante carbonates exhibit insignificant correlation with the detrital (siliciclastic) contents of samples (Fig. 6a,b), thus suggesting no detrital influence or overprint on the carbonate signatures. Although the influence of diagenetic alteration on the redistribution of some elements (e.g., Ca, Mg, Na, Mn, Fe, Sr, and Ba) in carbonates has been established (Veizer, 1983) and used for the evaluation of carbonate preservation in both Phanerozoic (e.g., Azmy et al., 1998; Veizer et al., 1999) and Precambrian sediments (Derry et al., 1992; Kaufman and Knoll, 1995), no detailed studies have yet investigated the fractionation of REE between carbonate phases during diagenesis. Diagenetic alteration is well known to cause significant depletion of Sr and enrichment of Mn in the diagenetic carbonate phase (Veizer, 1983) and the Mn/Sr ratio can be therefore used to evaluate the degree of carbonate preservation. The redox indicators utilized in the current study, Th/U and Ce/Ce* ratios, exhibit insignificant correlations with their Mn/Sr counterparts (Fig. 7a,b), thus suggesting a high degree of preservation of the Vazante REE signatures particularly for Th, U

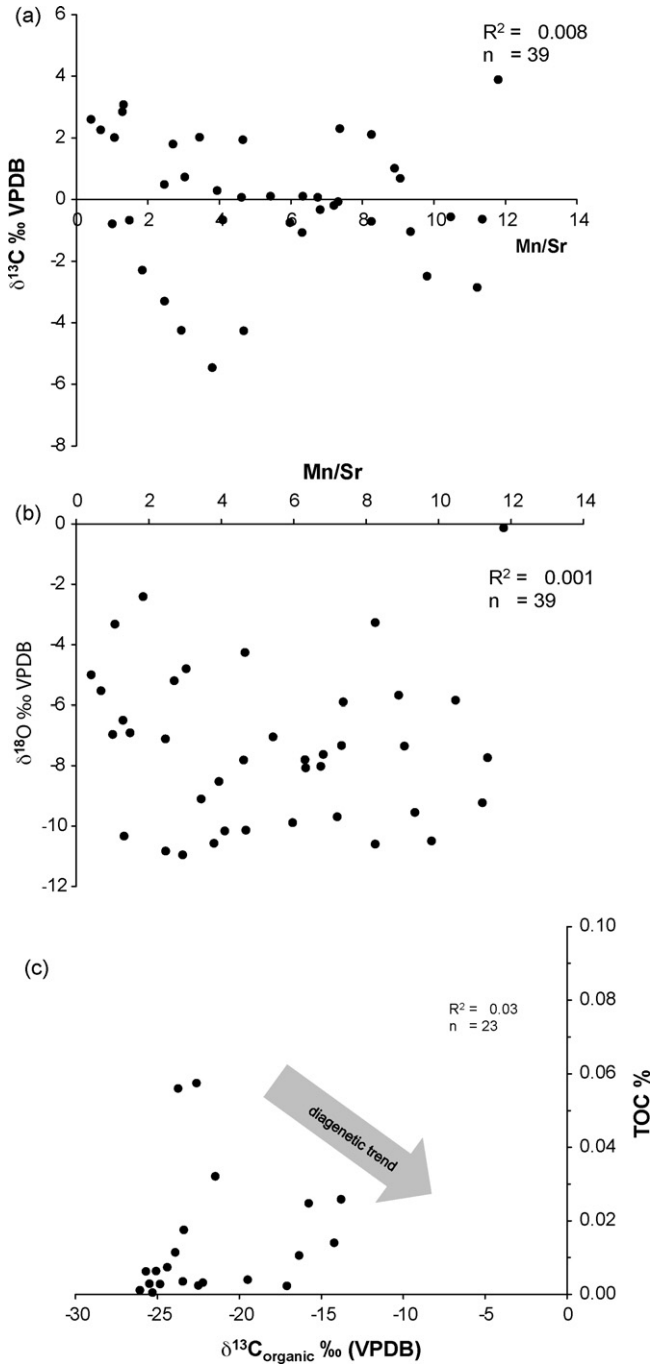

Fig. 4. Scatter diagrams of (a) Mn/Sr vs. $\delta^{13}C$, (b) Mn/Sr vs. $\delta^{18}O$, and (c) $\delta^{13}C$ vs. the total organic carbon contents (TOC) for dolomicrites (carbonate mud) of the upper Vazante Group showing lack of correlations.

and Ce. This is consistent with the correlation of the variations of those elements with their counterparts of the $\delta^{13}C$ of the Vazante carbonate and TOC profiles (Fig. 5).

The PAAS-normalized Vazante REE patterns (McLennan, 1989) also exhibit nearly parallel profiles through the studied sequence (e.g., Bau and Alexander, 2006) although some minor deviations may be observed in the Eu values (Fig. 8) but not in the Ce which is used as a redox indicator in the current study. In most parts of the sequence, the Vazante patterns are nearly similar to those averages of the modern microbialite and Pacific Ocean water (cf. Shields and Webb, 2004 and more reference therein) but they lack the negative Ce anomaly exhibited by the Pacific Ocean water (Fig. 8).

4.2. Redox conditions

Anoxic conditions have been known to be responsible for extinction events of biota or dramatic reduction in organic productivity during the Phanerozoic and Proterozoic (e.g., Erwin, 1993; Hoffman et al., 1998 and more references therein). Levels of oxygen in the water column, expressed as the redox conditions, influence the oxidation state of some elements and selectively control their solubility in seawater and consequently their degree of enrichment in marine sediments (e.g., Myers and Wignall, 1987; Wignall and Twitchett, 1996; Arnaboldi and Meyers, 2007; Wignall et al., 2007). Uranium is among the elements which are sensitive to redox conditions in seawater. In oxidizing environment, uranium ions maintain the higher oxidation state (U^{+6}) and form uranyl carbonate, which is soluble in water whereas in reducing conditions, they retain the lower oxidation state (U^{+4}) and form the insoluble uranous fluoride which is trapped into marine carbonates (Wignall and Twitchett, 1996). In contrast, thorium is not affected by the redox conditions of water column and occurs permanently in the insoluble Th^{+4} state. Accordingly, sediments of anoxic environments are richer in uranium and have lower Th/U than those of oxic environments. Therefore, the Th/U ratio has been used as a proxy for environmental redox conditions, with ratios < 2 in anoxic marine sediments, 2–7 in oxic sediments, and >7 in intensely oxidizing terrestrial environments (cf. Wignall and Twitchett, 1996).

The upper part of the Vazante Group has a distinct glaciogenic diamictite unit (D II) at the base of the Lapa Formation (Fig. 5), which is overlain by cap carbonates (Azmy et al., 2001, 2006; Misi et al., 2007). The $\delta^{13}C$ profile of the succession has remarkable primary shifts (Fig. 5) correlated with the stratigraphic levels immediately below and above the diamictite unit (Azmy et al., 2001, 2006). Recent Re–Os and U–Pb radiogenic-age studies give ages of ~1.0–1.1 Ga, suggesting that the Vazante Group was deposited during the late Mesoproterozoic (Azmy et al., 2008). Although the global $\delta^{13}C$ profile for late Mesoproterozoic cap carbonates is sparse (cf. Kah et al., 1999; Lindsay and Brasier, 2002; Bartley et al., 2007), comparable Neoproterozoic C-isotope shifts have been documented in association with global glacial events (cf. Halverson et al., 2005, 2007; Fike et al., 2007; Jiang et al., 2007 and more references therein) and can be utilized to shed the light on the depositional environment of the Vazante Basin.

The exact processes that might have resulted in large $\delta^{13}C$ shifts in marine sediments are still a matter of debate. The "Snowball Earth hypothesis" (e.g., Hoffman et al., 1998; Hoffman and Schrag, 2000) suggests that an extensive global glaciation during the Neoproterozoic reached at least near the paleoequatorial latitudes and isolated the ocean from atmosphere. The CO_2 evolved, in later stages, from volcanoes resulted in melting ice and initiated the precipitation of cap carbonates in ^{13}C-depleted oceans of low organic productivity but high alkalinity influx caused by enhanced weathering. Also, the postglacial ocean mixing and upwelling currents might have brought deep ^{12}C-rich water to shallow shelf environments which resulted in the precipitation of ^{13}C-depleted carbonates (e.g., Knoll et al., 1986; Kaufman et al., 1993; Grotzinger and Knoll, 1995). Alternatively, the released methane from exposed organic-rich sediments, by drop in sea level during glaciation, was trapped as methane hydrate in permafrost. The postglacial warming and sea level rise released methane in shelf water which resulted in the precipitation of ^{13}C-depleted carbonates (Kennedy et al., 2001).

On the other hand, C-isotope shifts have been documented in preglacial carbonates and were also attributed to a possible release

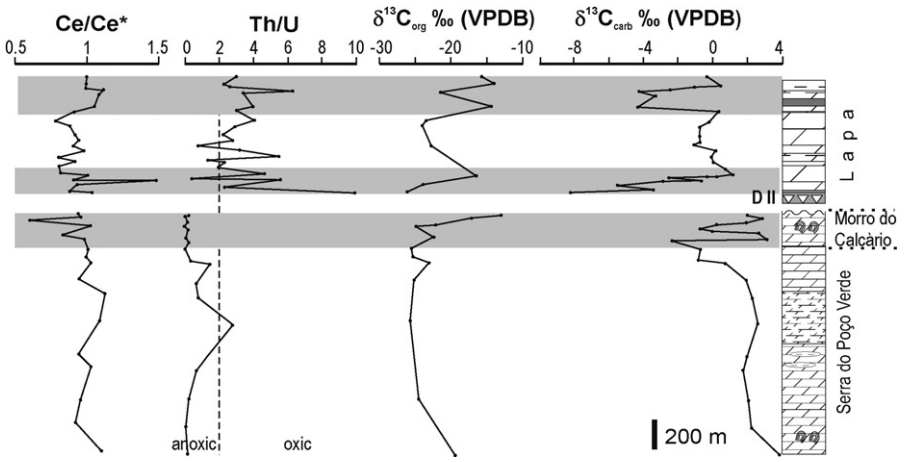

Fig. 5. Composite diagram showing the $\delta^{13}C_{carb}$, $\delta^{13}C_{org}$, Th/U and Ce/Ce* profiles of the upper Vazante carbonates (details in text). Legend as in Fig. 3.

of methane from organic-rich sediments on continental margins (Halverson et al., 2002; Schrag et al., 2002).

The $\delta^{13}C_{carb}$ profile of the upper Vazante (Fig. 5) exhibits two major different baselines, below and above the basal Lapa diamictite (D II). The preglacial baseline occurs at ~3‰ and the postglacial baseline at ~0‰ (VPDB), respectively (Fig. 5). Although variations in Precambrian seawater carbon budget can be, at times, attributed to paleoceanographic patterns (e.g., Knoll et al., 1986; Kaufman et al., 1993; Grotzinger and Knoll, 1995), the sedimentological evidence suggests that the Vazante carbonates were mainly deposited in a shallow marine platform setting (Dardenne, 1978; Dardenne and Walde, 1979; Madalosso, 1979; Karfunkel and Hoppe, 1988; Fairchild et al., 1996; Azmy et al., 2001; Dardenne, 2001; Misi, 2001,

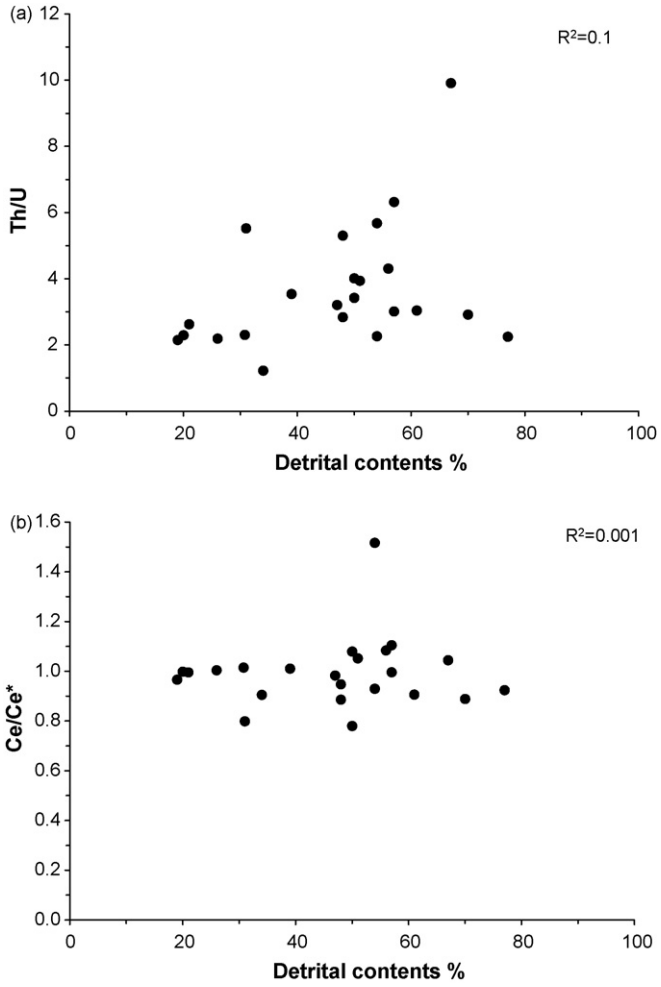

Fig. 6. Scatter diagrams of the detrital contents vs. (a) Th/U and (b) Ce/Ce* in the investigated Vazante carbonates exhibiting insignificant correlation. Detail in text.

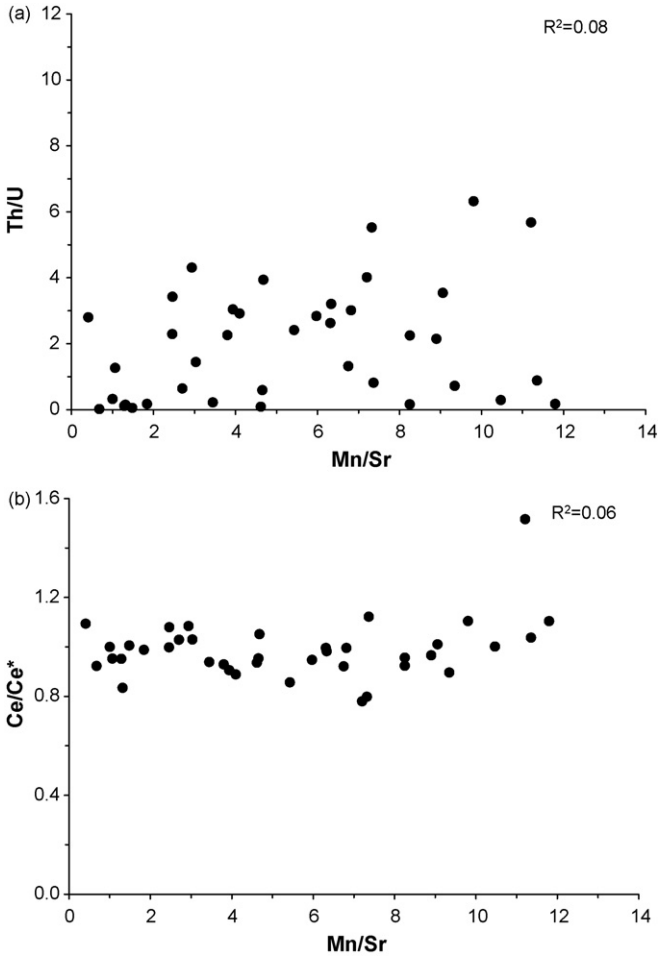

Fig. 7. Scatter diagrams of Mn/Sr vs. (a) Th/U and (b) Ce/Ce* showing insignificant correlations. See text for detail.

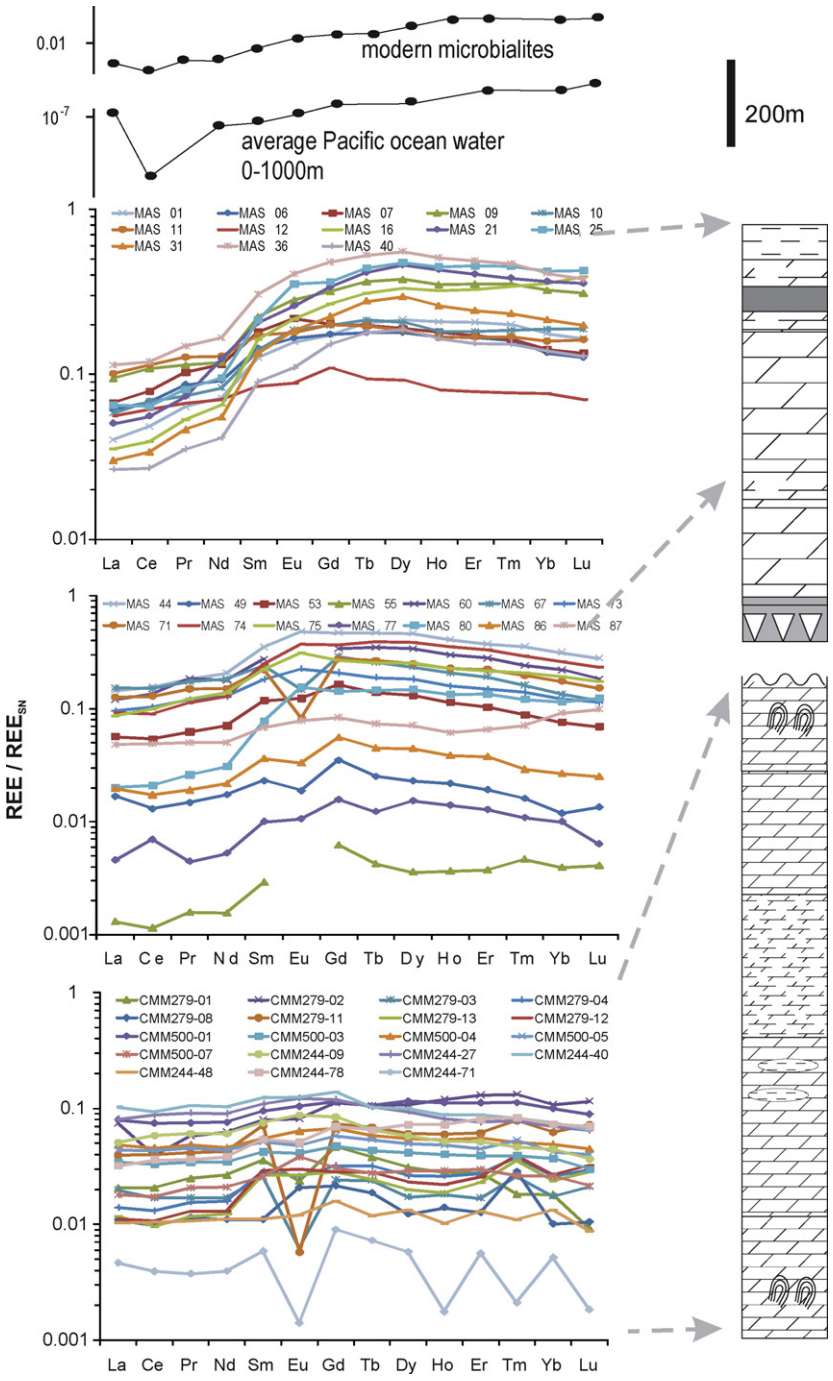

Fig. 8. The PAAS-normalized REE distribution patterns in the upper Vazante carbonates (McLennan, 1989). The modern microbialite and Pacific Ocean water patterns are modified from Shields and Webb (2004 and more references therein). The plotted results cover the stratigraphic zones of the three remarkable $\delta^{13}C_{carb}$ plunges below and above the diamictites (D II).

Misi et al., 2007). Therefore, the general long-term decrease in the $\delta^{13}C_{carb}$ of cap carbonates (Fig. 5) might reflect the impact of glaciation on the abundance and primary productivity of microbial biota in the postglacial Vazante Ocean. Excluding the $\delta^{13}C_{carb}$ values of swings associated with glacial events, the global C-isotope signatures of the Neoproterozoic carbonates (cf. Halverson et al., 2005, 2007) show generally more enriched values (around 5‰ VPDB) compared with those of the Vazante carbonates (around 0‰ VPDB), which may suggest that the evolution and abundance of microorganisms in late Mesoproterozoic oceans might have increased with time towards the late Neoproterozoic. However, this needs further study as relatively high $\delta^{13}C_{carb}$ values, up to 4‰ VPDB, have been recently documented for some older carbonate muds (late Mesoproterozoic – Middle Riphean) from the Avzyan Formation of southern Urals, Russia (Bartley et al., 2007).

The upper Vazante $\delta^{13}C_{carb}$ profile shows three major primary plunges towards isotopically lighter carbon (Fig. 5), a preglacial decrease of ~5‰ in mainly stromatolite-rich carbonates and microbial laminites (Azmy et al., 2001) immediately before the basal Lapa diamictite (D II) and two postglacial plunges of ~8‰ and ~5‰ in cap carbonate rhythmites after glaciation (Azmy et al., 2006). The lower postglacial plunge occurs immediately above the diamictite

unit and the upper plunge is associated with a shale layer at the top of the Lapa Formation (Fig. 5).

The preglacial shift (~5‰) correlates with Th/U values of 0.1–1.4 (Fig. 5) and thus is associated with precipitation of carbonates in reducing (anoxic–dysoxic) conditions (Th/U ≤ 2). The association of the reducing conditions with the preglacial negative $\delta^{13}C_{carb}$ is consistent with possible release of methane from organic-rich sediments on continental margins (e.g., Halverson et al., 2002; Schrag et al., 2002). However, the lack of a supporting sedimentological evidence (e.g., Jiang et al., 2003) in the Vazante carbonates, such as tube-like structures through which gas might have escaped (e.g., Hoffman and Schrag, 2002, Wang et al., 2008), might argue against the methane release scenario. Alternatively, the input of ^{12}C-enriched CO_2 in shelf environment might have been enhanced by sea level drop, caused by early regression preceding full glaciations, which brought some of the oxygen-restricted lower shelf water close to deep shelf settings rich in organic matter.

Unlike the positive correlations of the $\delta^{13}C_{carb}$ and Th/U profiles documented for the Permo-Triassic (e.g., Wignall and Twitchett, 1996) and Precambrian–Cambrian (Kimura and Watanabe, 2001) boundaries, those of the postglacial upper Vazante generally exhibit an opposite relationship (Fig. 5). The lower postglacial shift (~8‰) above the diamictite D II and the upper shift (~5‰) above the shale layer (Fig. 5) at the top of Lapa Formation (Azmy et al., 2001, 2006) correlate with Th/U values of 9.9–4.3, respectively, suggesting carbonate precipitation in oxidizing (Th > 2) environments.

The lower postglacial $\delta^{13}C_{carb}$ shift, immediately above the diamictite (D II), correlates with Th/U ratios that evolve from strongly reducing conditions (Th/U = 0.1) towards highly oxidizing conditions (Th/U = 9.9) and the signal continues upsection towards normal oxidizing conditions (Th/U = 2–6). The remarkable recovery in $\delta^{13}C_{carb}$ after the plunge (Fig. 5) likely reflects the combined effect of climate warming caused by high CO_2 input possibly from extensive volcanic activity, melting of ice caps, alkalinity influx and gradual increase in organic productivity. These factors would have triggered the precipitation of cap carbonates in ocean waters of low organic productivity (e.g., Kennedy et al., 2001; Halverson et al., 2002; Schrag et al., 2002). The highly oxic conditions (Th/U = 9.9), that immediately followed the termination of glaciations, might have been caused by the high solubility of oxygen in relatively cold water with initial restricted biota (cf. Olcott et al., 2005) and oxygen concentrations decreased with the progressive recovery of primary productivity after glaciation. Also, high Th/U ratios (>7) have been suggested to reflect terrestrial inputs (Wignall and Twitchett, 1996). The upper Vazante Th/U values (up to 9.9), correlated with stratigraphic levels immediately above the diamictite, are consistent with the argillaceous nature of the Lapa cap carbonates (rhythmites). This could reflect the effect of differential input of weathered continental materials due to possible fluctuations in the sea level during the initial stages of ice melting. However, the lack of correlation between the $\delta^{13}C_{carb}$ and the amount of carbonate in the samples suggests that the terrestrial input did not have enough organic matter to significantly influence the $\delta^{13}C$ signatures (Azmy et al., 2006).

The uppermost postglacial negative $\delta^{13}C_{carb}$ shift (~5‰) is recorded in rhythmites of laminated argillaceous carbonates (Azmy et al., 2006) overlying a shale layer and correlates with Th/U ratios (~2.3–6.3) of oxic conditions (Fig. 5). The upward passage of shale to carbonate rhythmites may indicate the onset of a sedimentary cycle of progressive shallowing after platform drowning, which might have resulted in a recovery in the primary productivity.

The upper Vazante Ce/Ce^* profile shows a similar trend to that of Th/U (Fig. 5). The preglacial $\delta^{13}C_{carb}$ plunge is correlated with a negative Ce/Ce^* shift of ~0.4, suggesting reducing conditions (e.g., Holser et al., 1989; Shields et al., 1997), which is consistent with their low (<2) Th/U values (Wignall and Twitchett, 1996; Wignall et al., 2007). In contrast, the lower postglacial plunge in $\delta^{13}C_{carb}$, immediately above the diamictite (D II), is correlated with a significant positive Ce/Ce^* shift of ~1.5 (Fig. 5), which reflects oxidizing conditions consistent with those suggested by the high Th/U ratios (>2). The upper postglacial drop in $\delta^{13}C_{carb}$ is correlated with only a weakly positive Ce/Ce^* shift of ~0.2. This implies oxidizing conditions consistent with those reflected by Th/U ratios at the same stratigraphic level. However, the lower Th/U and Ce/Ce^* values of the upper $\delta^{13}C_{carb}$ postglacial plunge, compared with their counterparts of the lower postglacial, and the lack of an immediate glaciogenic layer suggests that the uppermost $\delta^{13}C_{carb}$ was caused by a more localized oceanographic event rather than a major global climatic event. Generally speaking, the cap carbonates immediately above the diamictites (D II) show higher contents of Ce (Appendix A) compared with those of the preglacial carbonates and the uppermost carbonates above the topmost shale layer of the Lapa Formation (Fig. 3). This is consistent with the distinctive positive Ce/Ce^* shift associated with those cap carbonates.

5. Conclusions

The $\delta^{13}C$ profile of the late Mesoproterozoic upper Vazante Group carbonates, which include a glaciogenic diamictite unit, shows one preglacial and two (lower and upper) postglacial plunges towards isotopically lighter carbon. The isotopic decreases correlate with remarkable variations in the Th/U and Ce/Ce^* ratios, which reflect important redox variations in the Vazante Basin and possibly the late Mesoproterozoic ocean.

The preglacial $\delta^{13}C$ plunge (~5.4‰ VPDB) is associated with low Th/U ratios of <2 and a negative Ce/Ce^* shift of ~0.4, which suggests that those carbonates were deposited in reducing conditions. The drop of sea level preceding the glaciation probably resulted in consumption of oxygen through the oxidation of organic matter in the lower shelf environment and likely higher ^{12}C-input into the DIC reservoir.

In contrast, the postglacial plunges in $\delta^{13}C$ correlate with high Th/U ratios (>2) and increases in Ce/Ce^* (0.2–0.6), which reflect oxidizing conditions. The lower postglacial plunge (~9‰ VPDB), immediately above the diamictite layer, correlates with a very high Th/U ratio (~9.9) and a relatively strong increases in Ce/Ce^* (0.6) suggesting significant high oxidizing conditions. Oxidation developed as a result of the high solubility of atmospheric oxygen in relative cold water following ice melting during widespread deglaciation. The upper postglacial plunge in $\delta^{13}C$ (~4.6‰ VPDB), overlying a shale layer, correlates with a lower Th/U ratio (~6.3) and a weak increase in Ce/Ce^* (~0.2). This suggests a local oceanographic origin rather than a major global cooling event.

The results of this study indicate that both global and local climatic and oceanic changes produced large and abrupt redox variations in the oceans during the late Mesoproterozoic.

Acknowledgements

The authors wish to thank Dr. Alcides Nobrega Sial and anonymous reviewers for their constructive reviews and Votorantim Metais (Vazante, Minas Gerais, Brazil) for providing field assistance. This project was supported by funding from Memorial University of Newfoundland, Canada (to Karem Azmy), and by the Natural Sciences and Engineering Research Council of Canada (to Paul Sylvester).

Appendix A

Samples, description, sampled cores, stratigraphy, isotopic composition ($\delta^{18}O$ and $\delta^{13}C$ in ‰ VPDB), and trace element contents of the upper Vazante Group carbonates, more details in Azmy et al. (2001, 2006).

Sample id	Formation	Core	$\delta^{13}C$ ‰ VPDB	$\delta^{18}O$ ‰ VPDB	$\delta^{13}C_{organic}$ ‰ VPDB	TOC (%)	Detritals (%)	Depth (m)	Mn (ppm)	Sr (ppm)	La (ppb)	Ce (ppb)	Pr (ppb)	Nd (ppb)	Sm (ppb)	Eu (ppb)	Gd (ppb)	Tb (ppb)	Dy (ppb)	Ho (ppb)	Er (ppb)	Tm (ppb)	Yb (ppb)	Lu (ppb)	Th (ppb)	U (ppb)
MAS-01	Serra da Lapa Velosinho	MASW01	−0.3	−7.6	−15.8	0.02	57	54.9	232	34	1539	3856	562	2451	704	170	811	160	1006	207	591	81	500	72	391	130
MAS-06	Serra da Lapa Velosinho	MASW01	0.5	−7.1	−13.8	0.03	20	109.8	255	104	2356	5452	765	3117	798	180	816	138	840	167	477	65	380	55	440	192
MAS-07	Serra da Lapa Velosinho	MASW01	−1.1	−7.8			21	135.5	587	93	2570	6291	909	3894	1005	236	944	154	888	179	490	66	399	58	673	256
MAS-09	Serra da Lapa Velosinho	MASW01	−2.5	−10.5			57	158.6	2039	208	3617	8636	1005	4013	1238	305	1481	282	1765	347	1005	143	911	135	986	156
MAS-10	Serra da Lapa Velosinho	MASW01	−4.2	−11.0	−21.5	0.03	56	168.0	411	140	2221	5484	654	2816	779	201	920	165	963	180	516	75	530	81	1119	260
MAS-11	Serra da Lapa Velosinho	MASW01	−3.3	−10.8			50	179.2	207	84	3877	9101	1125	4370	959	194	934	152	871	166	481	69	449	70	2070	604
MAS-12	Serra da Lapa Velosinho	MASW01	−4.3	−10.1	−14.2	0.01	51	265.0	304	65	2142	4886	592	2398	471	96	511	73	431	80	224	31	216	31	728	185
MAS-15	Serra da Lapa Velosinho	MASW01	0.1	−8.7																						
MAS-16	Serra da Lapa Velosinho	MASW01	0.3	−8.5			61	299.7	319	81	1351	3111	471	2199	907	232	1242	240	1548	317	934	138	1003	169	282	93
MAS-21	Serra da Lapa Velosinho	MASW01	−0.2	−9.7	−23.4	0.02	50	363.5	497	69	1922	4438	647	4229	1146	280	1578	321	2156	428	1156	155	1033	154	989	246
MAS-25	Serra da Lapa Velosinho	MASW01	−0.7	−10.2	−23.9	0.01	70	405.8	578	141	2505	5113	717	3239	1188	381	1695	342	2226	445	1295	184	1194	184	463	159
MAS-31	Serra da Lapa Velosinho	MASW01	−0.7	−10.6			77	467.3	396	48	1152	2701	410	1869	746	198	1044	214	1382	257	692	95	601	86	361	160
MAS-36	Serra da Lapa Velosinho	MASW01	−0.8	−9.9			48	505.0	931	156	4355	9481	1306	5642	1694	438	2226	408	2592	503	1386	190	1153	163	955	336
MAS-40	Serra da Lapa Velosinho	MASW01	−1.0	−9.5	−22.6	0.06		539.3	691	74	1018	2157	312	1410	500	119	710	139	877	163	441	62	393	56	58	80
MAS-44	Serra da Lapa Velosinho	MASW01	0.1	−8.1			47	570.2	494	78	5539	12397	1622	7022	1942	520	2201	365	2177	407	1061	144	889	122	417	130
MAS-49	Serra da Lapa Velosinho	MASW01	−0.1	−7.3			31	614.5	637	87	641	1033	131	586	128	20	164	20	107	22	55	6	33	6	16	3
MAS-53	Serra da Lapa Velosinho	MASW01	0.1	−8.0				645.4	688	102	2167	4319	552	2408	658	134	767	108	619	113	295	36	214	30	71	54
MAS-55	Serra da Lapa Velosinho	MASW01	0.1	−7.0				658.5	532	98	50	91	14	53	16		29	3	17	4	11	2	11	2	9	4
MAS-60	Serra da Lapa Velosinho	MASW01	0.7	−7.3			39	696.0	498	55	4593	10725	1636	6033	1528		1586	270	1594	296	798	98	621	79	537	152
MAS-67	Serra da Lapa Velosinho	MASW01	1.0	−5.7			19	738.2	383	43	5867	12044	1541	6216	1341	159	1358	201	1103	207	548	66	383	51	334	155
MAS-71	Serra da Lapa Velosinho	MASW01	0.2	−6.1			26	755.0			4827	10298	1321	5111	1230	89	1295	207	1173	226	635	80	494	66	289	132
MAS-73	Serra da Lapa Velosinho	MASW01	−0.3	−5.8	−16.4	0.01	31	760.3			3658	8230	1063	4333	1014	244	972	147	861	158	426	57	344	50	226	98
MAS-74	Serra da Lapa Velosinho	MASW01	−2.5	−6.9			34	767.0			3503	7146	994	4328	1385	404	1733	306	1832	353	955	120	739	101	333	272
MAS-75	Serra da Lapa Velosinho	MASW01	−0.6	−5.8				777.2	278	27	3331	7963	1082	4718	1228	337	1257	198	1188	226	620	85	542	76	359	1221
MAS-77	Serra da Lapa Velosinho	MASW01	−2.9	−9.2			54	792.1	1143	102	173	552	39	178	55	11	73	9	72	14	37	4	28	3	40	7
MAS-80	Serra da Lapa Velosinho	MASW01	−5.5	−10.6	−23.7	0.06	54	827.6	646	170	771	1679	231	1046	429	169	668	114	694	133	385	49	326	54	41	18
MAS-86	Serra da Lapa Velosinho	MASW01	−3.4	−8.9	−23.4	0.00	48	848.7			751	1376	169	737	201	36	261	35	208	38	108	12	75	11	40	7
MAS-87	Serra da Lapa Velosinho	MASW01	−8.2	−9.4	−26.1	0.00	67	865.2			1848	3906	442	1702	380	85	390	57	334	61	187	29	259	43	735	74

Appendix A (*Continued*)

Sample id	Formation	Core	$\delta^{13}C$ ‰ VPDB	$\delta^{18}O$ ‰ VPDB	$\delta^{13}C_{organic}$ ‰ VPDB	TOC (%)	Detritals (%)	Depth (m)	Mn (ppm)	Sr (ppm)	La (ppb)	Ce (ppb)	Pr (ppb)	Nd (ppb)	Sm (ppb)	Eu (ppb)	Gd (ppb)	Tb (ppb)	Dy (ppb)	Ho (ppb)	Er (ppb)	Tm (ppb)	Yb (ppb)	Lu (ppb)	Th (ppb)	U (ppb)
CMM279-01	Morro do Càlcario	CMM279	2.9	−6.5	−17.1	0.00		92.0	90	70	786	1638	220	903	197	25	217	29	145	28	79	7	51	4	18	157
CMM279-02	Morro do Càlcario	CMM279	2.0	−7.5				118.0			2842	3091	508	2114	443	88	520	82	501	118	370	53	302	50	32	176
CMM279-03	Morro do Càlcario	CMM279	0.3	−4.7	−22.2	0.00		141.0			756	1346	149	575	143	7	113	19	81	18	48	10	49	9	58	370
CMM279-04	Morro do Càlcario	CMM279	0.1	−7.8				165.0	72	16	530	1037	137	538	158	28	150	25	123	26	78	15	74	13	42	467
CMM279-05	Morro do Càlcario	CMM279	1.7	−4.1				193.0	185	37																
CMM279-08	Morro do Càlcario	CMM279	2.0	−9.1	−13.0			80.0	141	41	415	783	101	373	61	22	101	15	57	14	36	12	28	5	24	109
CMM279-11	Morro do Càlcario	CMM279	−0.6	−7.7	−24.8	0.00		151.0	372	33	1498	3193	365	1444	394	6	343	53	283	59	174	32	175	32	385	435
CMM279-12	Morro do Càlcario	CMM279	2.7	−6.9				188.0			425	853	114	442	163	32	133	22	108	22	73	16	75	14	138	240
CMM279-13	Morro do Càlcario	CMM279	3.1	−10.3	−22.5	0.00		212.0	31	24	446	758	103	419	149	29	133	19	93	19	66	14	68	12	77	513
CMM500-01	Serra de Poço Verde	CMM500	−2.3	−2.4				32.0	128	70	3039	5921	662	2583	528	113	532	82	541	111	319	45	282	39	262	1475
CMM500-03	Serra de Poço Verde	CMM500	−0.7	−6.9	−25.5	0.00		76.0	60	41	1304	2629	303	1168	233	44	220	33	194	40	111	16	104	13	224	4142
CMM500-04	Serra de Poço Verde	CMM500	−0.8	−7.0	−25.3	0.00		138.0	38	38	1837	3614	427	1551	303	69	313	45	255	53	159	21	138	19	304	938
CMM500-05	Serra de Poço Verde	CMM500	0.7	−4.8	−23.1			173.0	148	49	1672	3434	401	1474	284	52	270	42	232	48	127	22	119	17	295	204
CMM500-07	Serra de Poço Verde	CMM500	1.9	−4.3	−25.1	0.01		286.0	202	43	688	1382	182	712	142	41	143	21	134	29	85	11	73	9	108	181
CMM244-09	Serra de Poço Verde	CMM244	2.3	−5.9				96.0	338	46	1941	4634	534	2063	419	95	393	50	271	52	146	19	125	16	257	315
CMM244-27	Serra de Poço Verde	CMM244	2.6	−5.0	−25.7	0.01		263.0	20	48	3085	6999	809	3053	605	133	559	80	441	81	219	32	198	28	505	180
CMM244-40	Serra de Poço Verde	CMM244	2.0	−3.3				480.7	69	65	3931	7496	941	3504	692	135	647	79	469	88	251	33	215	29	311	245
CMM244-48	Serra de Poço Verde	CMM244	1.8	−5.2				566.0	101	37	395	832	94	377	62	13	74	9	62	10	37	4	37	4	89	137
CMM244-61	Serra de Poço Verde	CMM244	2.1	−3.3	−24.4	0.01		756.0	392	48	982	1753	197	693	127	13	159	19	128	26	84	10	56	8	128	781
CMM244-71	Serra de Poço Verde	CMM244	2.3	−5.5				919.0	19	28	177	311	33	134	32	2	42	6	27	2	16	1	15	1	10	520
CMM244-78	Serra de Poço Verde	CMM244	3.9	−0.1	−19.5	0.00		11000	823	70	1222	2866	320	1294	300	55	327	51	339	72	230	34	207	30	169	968

References

Arnaboldi, M., Meyers, P.A., 2007. Trace element indicators of increased primary production and decreased water-column ventilation during deposition of latest Pliocene sapropels at five locations across the Mediterranean Sea. Palaeogeography, Palaeoclimatology, Palaeoecology 249, 425–443.

Arnold, G.L., Anbar, A.D., Barling, J., Lyons, T.W., 2004. Molybdenum isotope evidence for widespread anoxia in mid-Proterozoic oceans. Science 304, 87–90.

Azmy, K., Kaufman, A.J., Misi, A., Oliveira, T.F., 2006. Isotope stratigraphy of the Lapa Formation, São Francisco Basin, Brazil: implications for Late Neoproterozoic glacial events in South America. Precambrian Research 149, 231–248.

Azmy, K., Kendall, B., Creaser, R.A., Heaman, L., de Oliveira, T.F., 2008. Global correlation of the Vazante Group, São Francisco Basin, Brazil: Re–Os and U–Pb radiometric age constraints. Precambrian Research 164, 160–172.

Azmy, K., Veizer, J., Bassett, M.G., Copper, P., 1998. Oxygen and carbon isotopic composition of Silurian brachiopods: implications for coeval seawater and glaciations. Geological Society of America Bulletin 110, 1499–1512.

Azmy, K., Veizer, J., Misi, A., Oliveira, T.F., Sanches, A.L., Dardenne, M.A., 2001. Dolomitization and isotope stratigraphy of the Vazante formation, São Francisco Basin, Brazil. Precambrian Research 112, 303–329.

Bartley, J.K., Kah, L.C., McWilliams, J.L., Stagner, A.F., 2007. Carbon isotope chemostratigraphy of the Middle Riphean type section (Avzyan Formation, Southern Urals, Russia): signal recovery in a fold-and-thrust belt. Chemical Geology 237, 211–232.

Bau, M., Alexander, B., 2006. Preservation of primary REE patterns without Ce anomaly during dolomitization of Mid-Paleoproterozoic limestone and the potential re-establishment of marine anoxia immediately after the "Great Oxidation Event". South African Journal of Geology 109, 81–86.

Brocks, J.J., Love, G.D., Summons, R.E., Knoll, A.H., Logan, G.A., Bowden, S.A., 2005. Biomarker evidence for green and purple sulphur bacteria in a stratified Palaeoproterozoic sea. Nature 437, 866–870.

Brody, K.B., Kaufman, A.J., Eigenbrode, J., Cody, J., 2004. Biomarker geochemistry of a post-glacial Neoproterozoic succession in Brazil. In: Abstract, Geological Society of America Annual Meeting, Denver, CO, 7 to 10 November, 2004.

Campos-Neto, M.C., 1984. Litoestratigrafia, relações estratigráficas e evolução paleogeográfica dos grupos Canastra e Paranoá (região Vazante-Lagamar, MG). Revista Brasileira de Geociências 14, 81–91.

Coleman, M.L., Walsh, J.N., Benmore, R.A., 1989. Determination of both chemical and stable isotope composition in milligram-size carbonate samples. Sedimentary Geology 65, 233–238.

Dardenne, M.A., 1978. Sentese sobre a estratigrafiado Groupo Bambuí no Brasil Central. Trigésimo Congresso Brasileiro de Geologia 2, 597–610.

Dardenne, M.A., 2000. The Brasilia fold belt. In: Cordani, U.G., Milani, E.J., Thomaz-Filho, A., Campos, D.A. (Eds.), Tectonic Evolution of South América. 31st International Geological Congress. Rio de Janeiro, pp. 231–263.

Dardenne, M.A., 2001. Lithostratigraphic sedimentary sequences of the Vazante Group. In: IGCP 450 Proterozoic Sediment-Hosted Base Metal Deposits Of Western Gondwana (Abstr.), Belo Horizonte, Brazil, pp. 48–50.

Dardenne, M.A., Walde, D.H.G., 1979. A estratigrafia dos Grupos Bambuí e Macaúbas no Brasil Central. Bol. Soc. Bras. Geol., Núcleo Minas Gerais 1, 43–53.

Derry, L.A., Kaufman, A.J., Jacobsen, S.B., 1992. Sedimentary cycles and environmental change in the Late Proterozoic: evidence from stable and radiogenic isotopes. Geochimica Cosmochimica Acta 56, 1317–1329.

Dickson, J.A.D., 1966. Carbonate identification and genesis as revealed by staining. Journal of Sedimentary Petrology 36, 491–505.

Erwin, D.H., 1993. The Great Paleozoic Crisis. Columbia University Press, New York, p. 327.

Fairchild, T.R., Schopf, J.W., Shen-Miller, J., Guimarães, E.M., Edwards, M.D., Lagstein, A., Li, X., Pabst, M., De Melo-Filho, L.S., 1996. Recent discoveries of Proterozoic microfossils in south-central Brazil. Precambrian Research 80, 125–152.

Fike, D.A., Grotzinger, J.P., Pratt, L.M., Summons, R.E., 2007. Oxidation of the Ediacaran Ocean. Nature 444, 744–747.

Fuck, R.A., Pimentel, M.M., Silva, J.H.D., 1994. Compartimentação tectônica na porção oriental da Província Tocantins. In: 38° Congresso Brasileiro de Geologia, Camboriú–Sociedade Brasileira de Geologia, vol. 1, Anais, pp. 215–216.

Geboy, N.J., 2006. Rhenium-osmium age determinations of glaciogenic shales, Vazante Formation, Brazil. Unpublished M.Sc. Thesis, University of Maryland, College Park.

Grotzinger, J.P., Knoll, A.H., 1995. Anomalous carbonate precipitates: is the Precambrian the key to the Permian? Palaios 10, 578–596.

Halverson, G.P., Hoffman, P.F., Schrag, D.P., Maloof, A.C., Rice, A.H.N., 2005. Toward a Neoproterozoic composite carbon-isotope record. Geological Society of America Bulletin 117, 1181–1207.

Halverson, G.P., Maloof, A.C., Schrag, D.P., Dudás, F.Ő., Hurtgen, M., 2007. Stratigraphy and geochemistry of a ca 800 Ma negative carbon isotope interval in northeastern Svalbard. Chemical Geology 237, 5–27.

Halverson, G.P., Hoffman, P.F., Schrag, D.P., Kaufman, A.J., 2002. A major perturbation of the carbon cycle before the Ghaub glaciation (Neoproterozoic) in Namibia: Prelude to snowball Earth?: Geochemistry, Geophysics, Geosystems, 3, 24 p., doi:10.1029/2001GC000244.

Hayes, J.M., Kaplan, I.R., Wedeking, K.W., 1983. Precambrian organic geochemistry; preservation of the record. In: Schopf, J. (Ed.), Earth's Earliest Biosphere; its Origin and Evolution. Princeton University Press, Princeton, NJ, United States, pp. 93–134.

Hayes, J.M., Strauss, H., Kaufman, A.J., 1999. The abundance of ^{13}C in marine matter and isotopic fractionation in the global biogeochemical cycle of carbon during the past 800 Ma. Chemical Geology 161, 103–125.

Hoffman, P.F., Schrag, D.P., 2000. Snowball earth. Scientific American 282 (1), 68–75.

Hoffman, P.F., Schrag, D.P., 2002. The Snowball Earth hypothesis: testing the limits of global change. Terra Nova 14, 129–155.

Hoffman, P.F., Kaufman, A.J., Halverson, G.P., Schrag, D.P., 1998. A Neoproterozoic snowball Earth. Science 281, 1342–1346.

Holser, W.T., Schidlowski, M., Mackenzie, F.T., Maynard, J.B., 1988. Geochemical cycles of carbon and sulfur. In: Gregor, C.B., Garrels, R.M., Mackenzie, F.T., Maynard, J.B. (Eds.), Chemical Evolution of the Earth. Wiley, pp. 105–173.

Holser, W.T., Schönlaub, H.-P., Attrip Jr., M., Boeckelmann, K., Klein, P., Magaritz, M., Orth, C.J., Fenninge, A., Jenny, C., Kralik, M., Mauritsch, H., Pak, E., Schramm, J.-M., Stattegger, K., Schmoeller, R., 1989. A Unique geochemical record at the permian/Triassic Boundary. Nature 337, 39–44.

Jiang, G., Kaufman, A.J., Christie-Blick, N., Zhang, S., Wu, H., 2007. Carbon isotope variability across the Ediacaran Yangtze platform in South China: implications for a large surface-to-deep ocean $\delta^{13}C$ gradient. Earth and Planetary Science Letters 261, 303–320.

Jiang, G., Kennedy, M.J., Christie-Blick, N., 2003. Stable isotopic evidence for methane seeps in Neoproterozoic postglacial cap carbonates. Nature 426, 822–826.

Kah, L.C., Sherman, A.G., Narbonne, G.M., Knoll, A.H., Kaufman, A.J., 1999. $\delta^{13}C$ stratigraphy of the Proterozoic Bylot Supergroup, Baffin Island, Canada: implications for regional lithostratigraphic correlations. Canadian Journal of Earth Sciences 36, 313–332.

Kaufman, A.J., Geboy, N., Walker, R., Miller, K., Sievers, N., Poulton, S., de Oliviera, T., Misi, A., 2008. Re–Os ages of black shale in the glaciogenic Vazante Group: evidence for Mesoproterozoic ice ages in Brazil? (Abstract). IGC meeting, Oslo, August 2008. http://abstracts.congrex.com/scripts/JMEvent/ProgrammeLogic_Abstract_P.asp?PL=Y&Form_Id=8&Client_Id='CXST'&Project_Id='08080845'&Person_Id=1304439.

Karfunkel, J., Hoppe, A., 1988. Late Proterozoic glaciation in central-eastern Brazil: synthesis and model. Palaeogeography, Palaeoclimatology, Palaeoecology 65, 1–21.

Kaufman, A.J., Hayes, J.M., Knoll, A.H., Germs, G.J.B., 1991. Isotopic compositions of carbonates and organic carbon from upper Proterozoic successions in Namibia: stratigraphic variation and the effect of diagenesis and metamorphism. Precambrian Research 49, 301–327.

Kaufman, A.J., Jacobsen, S.B., Knoll, A.H., 1993. The Vendian record of Sr- and C-isotopic variations in seawater: implications for tectonics and paleoclimate. Earth Planetary Science Letters 120, 409–430.

Kaufman, A.J., Knoll, A.H., 1995. Neoproterozic variations in the C-isotopic composition of seawater: stratigraphic and biogeochemical implications. Precambrian Research 73, 27–49.

Kaufman, A.J., Knoll, A.H., Awramik, S.M., 1992. Biostratigraphic and chemostratigraphic correlation of Neoproterozoic sedimentary successions: upper Tindir Group, northwestern Canada, as a test case. Geology 20, 181–185.

Kennedy, M.J., Christie-Blick, N., Sohl, L.E., 2001. Are Proterozoic cap carbonates and isotopic excursions a record of gas hydrate destabilization following Earth's coldest intervals? Geology 29 (5), 443–446.

Kimura, H., Watanabe, Y., 2001. Oceanic anoxia at the Precambrian–Cambrian boundary. GSA Bulletin 29 (11), 995–998.

Knoll, A.H., Hayes, J.M., Kaufman, A.J., Swett, K., Lambert, I.B., 1986. Secular variations in carbon isotope ratios from Upper Proterozoic successions of Svalbard and East Greenland. Nature 321, 832–838.

Lindsay, J.F., Brasier, M.D., 2002. Did global tectonics drive early biosphere evolution? Carbon isotope record from 2.6 to 1.9 Ga carbonates of Western Australian basins. Precambrian Research 114, 1–34.

McLennan, S.M., 1989. Rare earth elements in sedimentary rocks: influence of provenance and sedimentary processes. In: Lipin, B.R., McKay, G.A. (Eds.), Geochemistry and Mineralogy of Rare Earth Elements, vol. 21. Mineral. Soc. Am. Rev. Miner., pp. 169–200.

Madalosso, A., 1979. Stratigraphy and sedimentation of the Bambuí Group in Paracatu region, Minas Gerais, Brazil. MSc. Thesis, University of Missouri, 127 p.

Misi, A., 2001. Estratigrafia isotópica das seqüências do Supergrupo São Francisco coberturas neoproterozócias do craton do São Francisco. Idade e correlacoes. In: C.P. Pinto, M.A. Martins-Neoto (Eds.), Bacia do São Francisco. Geologia e Recursos Naturais. SBG-Minas Gerais, pp. 67–92.

Misi, A., Kaufman, A.J., Veizer, J., Powis, K., Azmy, K., Boggiani, P.C., Gaucher, C., Teixeira, J.B.G., Sanches, A.L., Iyer, S.S., 2007. Chemostratigraphic correlation of Neoproterozoic successions in South America. Chemical Geology 237, 143–167.

Misi, A., Veizer, J., 1998. Neoproterozoic carbonate sequences of the Una Group, Irecê Basin, Brazil: chemostratigraphy, age and correlations. Precambrian Research 89, 87–100.

Myers, K.J., Wignall, P.B., 1987. Understanding Jurassic organic-rich mudrocks-new concepts using gamma-ray spectrometry and palaeoecology: examples from the Kimmeridge Clay of Dorset and the Jet Rock of Yorkshire. In: Legget, J.K., Zuffa, G.G. (Eds.), Marine Clastic Sedimentology. Graham and Trotman, London, pp. 172–189.

Narbonne, G.M., Kaufman, A.J., Knoll, A.H., 1994. Integrated chemostratigraphy and biostratigraphy of the Windermere Supergroup, northern Canada: implications for Neoproterozoic correlations and early evolution of animals. GSA Bulletin 106, 1281–1292.

Olcott, A.N., Sessions, A.L., Corsetti, F.A., Kaufman, A.J., de Oliviera, T.F., 2005. Biomarker evidence for photosynthesis during Neoproterozoic glaciation. Science 310, 471–474.

Rush, P.F., Chafetz, H.S., 1990. Fabric retentive, non-luminescent brachiopods as indicators of original $\delta^{13}C$ and $\delta^{18}O$ compositions: a test. Journal of Sedimentary Petrology 60, 968–981.

Schidlowski, M., Eichmann, R., Junge, C.E., 1975. Precambrian sedimentary carbonates: carbon and oxygen isotope geochemistry and implications for the terrestrial oxygen budget. Precambrian Research 2, 1–69.

Schrag, D.P., Berner, R.A., Hoffman, P.F., Halverson, G.P., 2002. On the initiation of a snowball earth. Geophysics, Geochemistry, Geosystems 3 (6), doi:10-1029/2001GC000219.

Schen, Y., Canfield, D.E., Knoll, A.H., 2002. Middle Proterozoic ocean chemistry: evidence from the McArthur Basin, Northern Australia. American Journal of Science 302, 81–109.

Schen, Y., Knoll, A.H., Walter, M.R., 2003. Evidence for low sulphate and anoxia in a mid-Proterozoic marine basin. Nature 423, 632–635.

Shields, G.A., Stille, P., Brasier, M.D., Atudorei, V., 1997. Ocean stratification and oxygenation of the Late Precambrian environment: a post-glacial geochemical record from a Neoproterozoic section in W. Mongolia. Terra Nova 9, 218–222.

Shields, G.A., Webb, G.E., 2004. Has the REE composition of seawater changed over geological time? Chemical Geology 204, 103–107.

Valeriano, C.M., Dardenne, M.A., Fonseca, M.A., Simões, L.S.A., Seere, H.J., 2004. A evolução tectônica da Faixa Brasília. In: Mantesso-Neto, V., Bartorelli, A., Carneiro, C.D.R., Brito Neves, B.B. (Eds.), Geologia do Continente Sul Americano: Evolução da Obra de Fernando Flávio Marques de Almeida. Editora Beca, pp. 575–593.

Veizer, J., 1983. Chemical diagenesis of carbonates: theory and application of trace element technique. In: M.A. Arthur, T.F. Anderson, I.R. Kaplan, J. Veizer, L.S., Land (Eds.), Stable Isotopes in Sedimentary Geology. Society of Economic Paleontologists and Mineralogists (SEPM) Short Course Notes 10, III-1-III-100.

Veizer, J., Ala, D., Azmy, K., Bruckschen, P., Bruhn, F., Buhl, D., Carden, G., Diener, A., Ebneth, S., Godderis, Y., Jasper, T., Korte, C., Pawellek, F., Podlaha, O., Strauss, H., 1999. $^{87}Sr/^{86}Sr$, $\delta^{18}O$ and $\delta^{13}C$ evolution of Phanerozoic seawater. Chemical Geology 161, 59–88.

Wang, J., Jiang, G., Xiao, S., Li, Q., Wei, Q., 2008. Carbon isotope evidence for widespread methane seeps in the ca. 635 Ma Doushantuo cap carbonate in south China. Geology 36, 347–350.

Wignall, P.B., Twitchett, R.J., 1996. Oceanic anoxia and the end Permian mass extinction. Science 272, 1155–1158.

Wignall, P.B., Zonneveld, J.-P., Newton, R.J., Amor, K., Sephton, M.A., Hartley, S., 2007. The end Triassic mass extinction record of Williston Lake, British Columbia. Palaeogeography, Palaeoclimatology, Palaeoecology 253, 385–406.